Tompa-De Meulenaur analytical method. In addition to various local programs for the CDC 6600 computer, modified versions of the following were employed: MULTAN, direct method program of Main, Germain, and Woolfson, Zalkin's FORDAP Fourier summation program, Johnson's ORTEP thermal ellipsoid plotting program, and Busing's and Levy's ORFFE error function program. Our full-matrix least-squares program, NUCLS, in its nongroup form, closely resembles the Busing-Levy ORFLS program.
(17) Cromer, D. T.; Waber, J. T. "International Tables for X-ray Crystallography", Vol. IV; Kynoch Press: Birmingham, England, 1974; Table 2.2A. Cromer, D. T. *Ibid.*, Table 2.3.1.
(18) Stewart, R. F.; Davidson, E. R.; Simpson, W. T. *J. Chem. Phys.* **1965**, *42*, 3175-3179.
(19) Ibers, J. A.; Hamilton, W. C. *Acta Crystallogr.* **1964**, *17*, 781-782.
(20) See paragraph at end of paper regarding supplementary material.
(21) Green, M.; Laguna, A.; Spencer, J. L.; Stone, F. G. A. *J. Chem. Soc., Dalton Trans.* **1977**, 1010-1016.
(22) McClellan, W. R. *J. Am. Chem. Soc.* **1961**, *83*, 1598-1601.
(23) Tatlershall, B. W.; Resl, A. J.; Green, M.; Stone, F. G. A. *J. Chem. Soc.* **1968**, 899-902.
(24) Churchill, M. R.; DeBoer, B. G.; Shapley, J. R.; Keister, J. B. *J. Am. Chem. Soc.* **1976**, *98*, 2357-2358.
(25) Reger, D. L.; Dukes, M. D. *J. Organomet. Chem.* **1978**, *153*, 67-72.
(26) Fields, R.; Godwin, G. L.; Haszeldine, R. N. *J. Chem. Soc., Dalton Trans.* **1975**, 1867-1872.
(27) Hullner, G.; Garlzke, W. *Chem. Ber.* **1972**, *105*, 2714.
(28) Yamamoto, Y.; Aoki, K.; Yamazaki, H. *J. Am. Chem. Soc.* **1974**, *96*, 2647-2648.
(29) Dahl, L. F.; Wei, C. H. *Inorg. Chem.* **1963**, *2*, 328-333.
(30) Henslee, W.; Davis, R. E. *Cryst. Struct. Commun.* **1972**, *403*, 185.
(31) Coleman, J. M.; Wojcicki, A.; Pollick, P. J.; Dahl, L. F. *Inorg. Chem.* **1967**, *6*, 1236-1242.
(32) Le Borgne, G.; Grandjean, D.; Mathieu, R.; Poilblanc, R. *J. Organomet. Chem.* **1977**, *131*, 429-438.
(33) Savariault, J. M.; Bonnel, J. J.; Malhieu, R.; Galy, J. *C. R. Acad. Sci., Ser. C* **1977**, *284*, 663-665.
(34) Clegg, W. *Inorg. Chem.* **1976**, *15*, 1609-1613.

Structure of η^3-Cyclooctenyltris(trimethyl phosphite)iron(I). Bonding of the η^3-Alkenyl Group to 16-, 17-, and 18-Electron ML_3 Systems

R. L. Harlow, R. J. McKinney, and S. D. Ittel*

Contribution No. 2673 from the Central Research and Development Department, E. I. du Pont de Nemours and Company, Experimental Station, Wilmington, Delaware 19898. *Received June 13, 1979*

Abstract: The crystal and molecular structure of $Fe(\eta^3\text{-}C_8H_{13})(P(OMe)_3)_3$ has been determined at −80 °C by X-ray diffraction. The monoclinic crystals ($C2/c$) have unit cell dimensions a = 14.940 (3) Å, b = 11.626 (3) Å, c = 29.952 (5) Å, β = 103.88 (2)°, and V = 5050.5 Å^3. Full-matrix least-squares refinement led to $R(F_o)$ = 0.035 and $R_w(F_o)$ = 0.036. The coordination sphere about the iron atom is a distorted square pyramid if the η^3-cyclooctenyl group is considered to be a bidentate ligand. The η^3-allylic group is symmetrical but skewed with respect to the basal plane. This twisting allows a hydrogen atom on a carbon atom attached to the η^3-allylic group to have a very weak (2.77 (2) Å) interaction with the metal center. Extended Hückel theory, with the inclusion of two-body repulsion, has been used to reproduce molecular geometries, including bond lengths, of 16-, 17-, and 18-electron complexes of the type $[M(\eta^3\text{-alkenyl})(P(OMe)_3]^{+x}$. Barriers to several intramolecular rearrangements have been calculated for these species and agree well with NMR and ESR measurements. The bonding in the 16-, 17-, and 18-electron species is discussed.

Introduction

The dimeric species, $[Fe(\eta^3\text{-allyl})(CO)_3]_2$, prepared by a

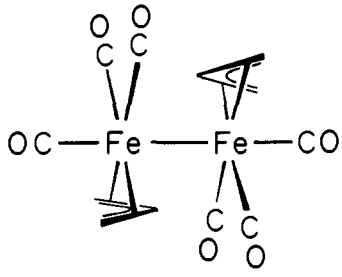

one-electron reduction of $FeX(\eta^3\text{-allyl})(CO)_3$ complexes (where X = halide), has been shown to exist in equilibrium with its paramagnetic monomer.[1-3] This monomer-dimer equilibrium is very sensitive to steric effects. Thus, if substituents are added to the allyl group,[1] or one or more of the carbonyl ligands are replaced with phosphorus ligands,[1,2] the equilibrium is shifted dramatically toward the monomeric species.

The phosphite complex $[Fe(\eta^3\text{-cyclooctenyl})(P(OMe)_3)_3][BF_4]$[4,5] (**1**) undergoes a similar one-electron reduction to give the monomeric species $Fe(\eta^3\text{-cyclooctenyl})(P(OMe)_3)_3$[6] (**2**). Complex **2** shows no tendency to form a

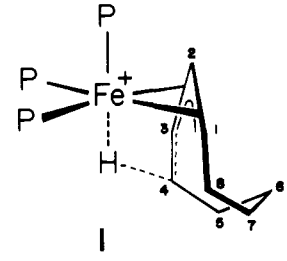

I

diamagnetic dimer. Additionally, it is fluxional on the ESR time scale, showing hyperfine coupling to three nonequivalent[7] phosphorus nuclei in slow exchange at −140 °C. As the system is warmed a dynamic process begins to equilibrate the two similar phosphorus nuclei until at −60 °C the spectrum appears as a doublet of triplets. As the system is warmed further, a second, independent fluxional process begins to equilibrate all three phosphorus nuclei, giving a quartet at 140 °C. While we were able to simulate the permutational behavior of the phosphorus nuclei, without some knowledge of the ground-state geometry, we were unable to draw any conclusions about the physical dynamic process related to that permutational behavior.

The crystal structure of the dimeric species $[Fe(\eta^3\text{-}C_3H_5)(CO)_3]_2$ has been reported,[3] but from spectroscopic measurements the solution structure of **2** is clearly of lower symmetry than would be expected for half of the dimer. Two

0002-7863/79/1501-7496$01.00/0 © 1979 American Chemical Society

Table I. Positional Parameters and Their Estimated Standard Deviations for Important Atoms in $Fe(P(OMe)_3)_3(\eta^3\text{-}C_8H_{13})$

atom	X	Y	Z	atom	X	Y	Z
Fe	0.207 47(2)	0.485 83(2)	0.363 48(1)	C(1)	0.1685(1)	0.5288(2)	0.290 89(7)
P(1)	0.291 27(4)	0.423 17(5)	0.426 10(2)	C(2)	0.2075(1)	0.4178(2)	0.301 14(7)
P(2)	0.086 13(4)	0.396 68(5)	0.371 45(2)	C(3)	0.2971(1)	0.3995(2)	0.328 66(7)
P(3)	0.178 09(4)	0.653 63(5)	0.386 12(2)	C(4)	0.3781(1)	0.4782(2)	0.328 40(8)
				C(5)	0.4036(2)	0.4861(2)	0.281 20(8)
O(11)	0.3976(1)	0.4645(2)	0.444 96(6)	C(6)	0.3237(2)	0.4945(2)	0.238 56(8)
O(12)	0.3125(1)	0.2868(1)	0.430 76(6)	C(7)	0.2610(2)	0.5999(2)	0.234 26(8)
O(13)	0.2496(1)	0.4391(2)	0.470 50(5)	C(8)	0.2198(2)	0.6284(2)	0.275 37(8)
O(21)	0.0870(1)	0.2629(1)	0.389 09(5)	C(11)	0.4206(2)	0.5848(2)	0.446 50(10)
O(22)	0.0087(1)	0.3894(1)	0.323 36(5)	C(12)	0.3946(2)	0.2318(3)	0.427 14(12)
O(23)	0.0270(1)	0.4465(1)	0.405 82(5)	C(13)	0.3008(2)	0.4060(3)	0.515 82(9)
O(31)	0.2016(1)	0.6892(1)	0.440 13(5)	C(21)	0.1251(2)	0.1779(2)	0.364 38(9)
O(32)	0.2397(1)	0.7540(1)	0.370 90(6)	C(22)	−0.0789(2)	0.3342(3)	0.319 42(10)
O(33)	0.0758(1)	0.7095(2)	0.373 13(6)	C(23)	0.0038(2)	0.3889(3)	0.442 69(9)
				C(31)	0.1415(2)	0.6665(3)	0.469 58(9)
H(8)A	0.267(2)	0.660(2)	0.2986(8)	C(32)	0.2294(2)	0.8724(2)	0.383 60(11)
H(4)B	0.366(2)	0.556(2)	0.3385(8)	C(33)	0.0157(2)	0.6924(2)	0.328 56(10)

recently reported structures[8,9] prompted us to choose **2** for an X-ray crystallographic study. The coordinatively saturated 18-electron system $Co(\eta^3\text{-cyclooctenyl})(P(OMe)_3)_3$ (**3**) is of

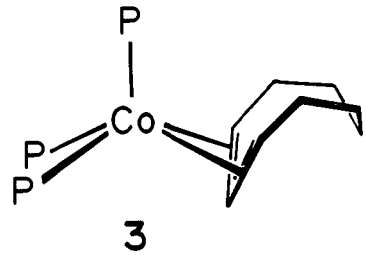

3

approximate square pyramidal geometry if the η^3-enyl system is considered to be a bidentate ligand.[8] The complex has close to mirror symmetry if one ignores the methoxy groups of the phosphite ligands.

The nominally 16-electron system $[Fe(\eta^3\text{-cyclooctenyl})(P(OMe)_3)_3][BF_4]$ (**1**) is of approximate octahedral geometry.[9] The endo hydrogen atom on C_4 (see configuration **1**) is bonded to the iron center in the vacant sixth coordination site. This Fe–H–C interaction coincides with a marked distortion of the η^3-enyl group and the remainder of the cyclooctenyl group.

With the structures of the 16- and 18-electron $M(\eta^3\text{-cyclooctenyl})(P(OMe)_3)_3$ complexes available for comparison, the structure of **2** is of great interest. Comparison of the bonding in the three species affords a better understanding of both the η^3-alkenyl bonding and the M–H–C interaction.

Extended Hückel theory, modified with the inclusion of two-body repulsion and geometry optimization (MEHT), has been used to reproduce and predict geometries of transition-metal complexes.[10] Calculated molecular energies can be related to enthalpies of activation for dissociative processes. These methods can be used to detail systems where modes of bonding are unclear.

Experimental Section

All work was carried out in the dry nitrogen atmosphere of a Vacuum Atmospheres drybox. Solvents were dried by conventional techniques and stored under nitrogen. The synthesis of $Fe(\eta^4\text{-cyclooctadiene})(P(OMe)_3)_3$[11] by metal-atom evaporation and its protonation to give $[Fe(\eta^3\text{-cyclooctenyl})(P(OMe)_3)_3][BF_4]$ (**1**)[4,5] have been reported. The reduction of **1** in tetrahydrofuran with sodium amalgam to yield the dark blue, paramagnetic species $Fe(\eta^3\text{-cyclooctenyl})(P(OMe)_3)_3$ (**2**) has also been reported.[6] Crystals of **2** were grown at −40 °C by slow evaporation of a hexane solution. Under nitrogen, the solution is stable at room temperature for over 2 years.

Preliminary film work indicated that the complex crystallizes in the monoclinic space group $C2/c$ [C_{2h}^6, no. 15] with eight molecules per unit cell.

A crystal of approximate dimensions 0.45 × 0.51 × 0.19 mm was sealed in a glass capillary and mounted on a Syntex P3 diffractometer in a random orientation. Graphite monochromated molybdenum Kα radiation (λ = 0.710 69 Å) was used, and the crystal was cooled to −80 °C in a stream of cold nitrogen. Unit cell dimensions and orientations were determined from the setting angles of 45 computer-oriented reflections: a = 14.940 (3) Å, b = 11.626 (3) Å, c = 29.952 (5) Å, β = 103.88 (2)°, and V = 5050.5 Å^3. The calculated density was 1.470 g cm^{-3}, based on eight molecules per unit cell. The width at half-height of ω scans was 0.25°. Data were collected by the ω scan technique at a rate of 2.0–5.0° min^{-1} over a scan range of 1.0°. The ratio of scan time to background counting time was 1.0. Data were collected from 2θ = 4° to 55° giving a total of 5802 independent reflections. The intensities of four standard reflections were checked every 200 reflections, and found to be satisfactory.

Lorentz and polarization corrections were applied. An absorption correction was made using the ψ-scan technique. Transmission factors based on μ = 8.46 cm^{-1} varied from 0.82 to 1.00.

The solution and refinement of the structure were carried out on a PDP-11 computer using local modifications of the programs supplied by the Enraf-Nonius Corp.[12] The atomic scattering factors were taken from the tabulations of Cromer and Waber;[13a] anomalous dispersion corrections were by Cromer.[13b] In the least-squares refinement, the function minimized was $\Sigma w(|F_o| - |F_c|)^2$ with the weights, w, assigned as $1/\sigma^2(F_o)$. The standard deviations of the observed structure factors, $\sigma(F_o)$, were based on counting statistics and an "ignorance factor," p, of 0.02.[14]

The structure was solved by direct methods. The positions of the hydrogen atoms were determined by Fourier difference techniques. Full-matrix least-squares refinement of all positional and thermal parameters (anisotropic for Fe, P, O, and C; isotropic for H) using the 4771 reflections with $F^2 > 2\sigma(F^2)$ converged at

$$R = \Sigma||F_o| - |F_c||/\Sigma|F_o| = 0.035$$

$$R_w = [\Sigma w(|F_o| - |F_c|)^2/\Sigma w|F_o|^2]^{1/2} = 0.036$$

A final difference Fourier map showed several peaks which ranged in magnitude from 0.5 to 0.9 e/Å^3. Several of these peaks were about 1.5 Å from phosphorus atoms in areas which could be alternate oxygen atom positions, indicating a minor disorder problem. The remaining peaks were associated with the phosphorus and iron atoms. Final positional parameters of nonhydrogen atoms are listed in Table I. Tables of anisotropic thermal parameters for nonhydrogen atoms, coordinates, and isotropic thermal parameters for hydrogen atoms, and observed and calculated structure factors have been submitted as supplementary material.[15]

Computational details for the use of MEHT have been described previously.[10] Atomic parameters were taken from literature sources[16-18] where they were approximated from experimental data.

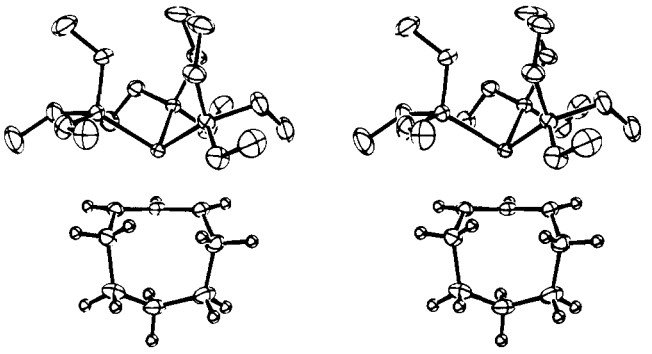

Figure 1. Stereoscopic view of $Fe(\eta^3\text{-}C_8H_{13})(P(OCH_3)_3)_3$ with phosphite hydrogen atoms omitted for clarity.

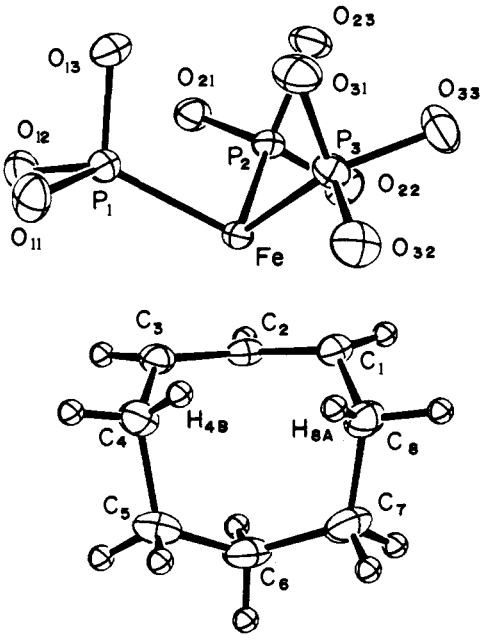

Figure 2. Atom labeling scheme for $Fe(\eta^3\text{-}C_8H_{13})(P(OCH_3)_3)_3$ with phosphite hydrogen atoms omitted for clarity. The thermal ellipsoids of nuclear motion for all nonhydrogen atoms are scaled to enclose 50% probability.

Results and Discussion of the Structure

The crystal structure consists of discrete $Fe(C_8H_{13})(P(OMe)_3)_3$ molecules. The shortest intermolecular contacts are those between hydrogen atoms of the methoxy groups. A stereoview is displayed in Figure 1; the atom numbering scheme is shown in Figure 2; pertinent bond distances and angles are given in Table II.

The structure of **2** is a distorted square pyramid (if the η^3-cyclooctenyl group is considered to be a bidentate ligand). The marked similarity between this structure and that of the cationic precursor, **1**, invites comparison. Figure 3 shows similar views of the inner coordination sphere of the 16-, 17-, and 18-electron systems (**1**, **2**, and **3**, respectively). The coordination geometry of **1** is octahedral with the three iron–phosphorus vectors mutually perpendicular. The P–Fe–P angles in **2** (P_1–Fe–P_2 = 94.06 (2), P_2–Fe–P_3 = 99.28 (2), and P_1–Fe–P_3 = 98.92 (2)°; P_2 is axial) have opened so that the coordination geometry is more square pyramidal. The P–Co–P angles in **3** are even larger than those observed in **2** with very noticeable differentiation of the apical–basal and basal–basal angles (103.5 (1), 106.2 (1), and 97.4 (1)°). There are no significant changes in the M–P distances in the three structures. The greatest difference between the structures of **1** and **2** and the structure of **3** is the orientation of the cyclooctenyl group. In **1** and **2** the nonallylic portion of the ring is oriented below the basal plane, but in **3** it is oriented above the plane. The orientation in **1** allows the octahedral coordination sphere to be completed by coordination of an aliphatic hydrogen atom of the cyclooctenyl group to the metal center (Fe–H = 1.95 (3) Å; 1.879 (9) Å by neutron diffraction).[9] A similar but much weaker interaction is observed in **2**; H_{4B} is 2.77 (2) Å from the iron atom below the basal plane. This distance is too long to be considered a bond but nonetheless is within the range of many previously cited metal–hydrogen "interactions".[19] No Co–H interactions are observed or expected in the coordina-

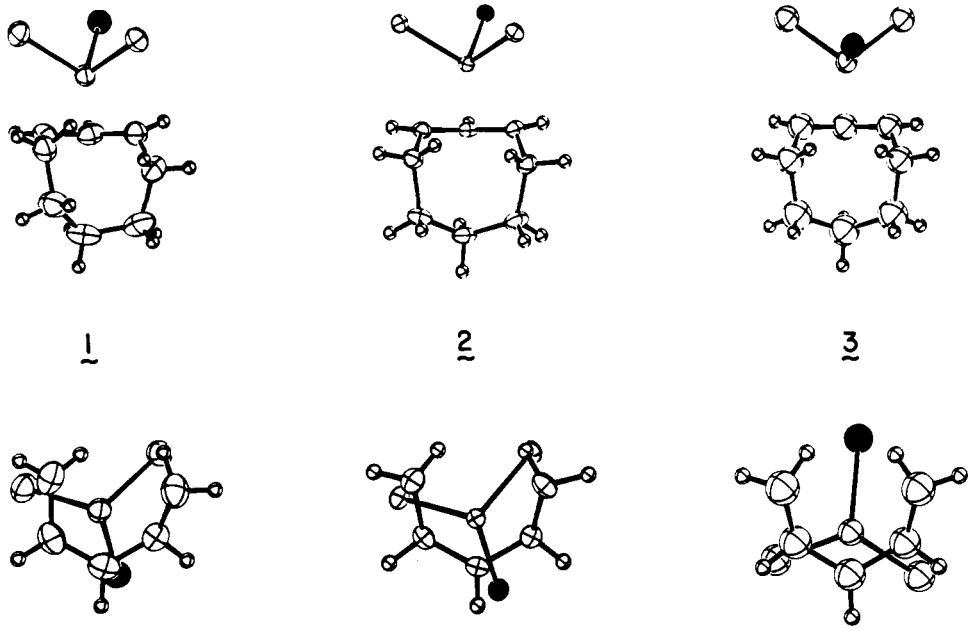

Figure 3. Inner coordination spheres of **1**, **2**, and **3** viewed perpendicular to $\overline{C_1C_3}$ of the allyl fragment. In the top three figures the viewer is in the allyl plane and the entire cyclooctenyl ring is shown. In the bottom three figures the viewer is perpendicular to the C_1–C_2–C_3 plane and C_5, C_6, and C_7 have been omitted for the sake of clarity. In the top figures, especially note the perturbation of the ring as H_4 moves toward the metal (going from **3** to **2** to **1**). In the bottom three figures note the orientation of the phosphorus ligands with respect to the allyl group. The axial ligand is darkened for clarity.

Table II. Selected Bond Distances and Angles in $Fe(P(OMe)_3)_3$ (η^3-C_8H_{13})

	Bond Distances (Å) with Estimated Standard Deviations		
Fe-P(1)	2.119(1)	P(2)-O(21)	1.641(1)
Fe-P(2)	2.151(1)	P(2)-O(22)	1.619(1)
Fe-P(3)	2.145(1)	P(2)-O(23)	1.616(1)
P(1)-O(11)	1.626(1)	P(3)-O(31)	1.625(1)
P(1)-O(12)	1.616(1)	P(3)-O(32)	1.617(1)
P(1)-O(13)	1.608(1)	P(3)-O(33)	1.620(1)
Fe-C(2)	2.028(2)	C(1)-C(8)	1.522(2)
Fe-C(1)	2.170(2)	C(3)-C(4)	1.519(2)
Fe-C(3)	2.135(2)	C(7)-C(8)	1.538(3)
Fe-C(8)	3.159(2)	C(4)-C(5)	1.552(2)
Fe-C(4)	2.983(2)	C(5)-C(6)	1.528(3)
Fe-H(8)A	3.08(2)	C(6)-C(7)	1.529(3)
Fe-H(4)B	2.77(2)	C(8)-H(8)B	1.05(2)
C(1)-C(2)	1.419(2)	C(8)-H(8)A	0.94(2)
C(2)-C(3)	1.410(2)	C(4)-H(4)A	0.93(2)
C(2)-H(2)	0.90(2)	C(4)-H(4)B	0.99(2)
C(1)-H(1)	0.96(2)	C(3)-H(3)	0.99(2)
	Bond Angles (deg) with Estimated Standard Deviations		
P(1)-Fe-P(2)	94.06(2)	P(1)-Fe-H(8)A	125.9(4)
P(2)-Fe-P(3)	99.28(2)	P(3)-Fe-H(8)A	73.3(4)
P(1)-Fe-P(3)	98.92(2)	P(1)-Fe-H(4)B	88.8(4)
P(1)-Fe-C(2)	123.39(5)	P(3)-Fe-H(4)B	94.0(4)
P(3)-Fe-C(2)	133.72(5)	P(2)-Fe-C(1)	101.02(5)
P(1)-Fe-C(1)	157.78(5)	P(2)-Fe-C(3)	118.15(5)
P(3)-Fe-C(3)	141.43(5)	P(2)-Fe-C(2)	95.75(5)
P(1)-Fe-C(3)	87.95(5)	P(2)-Fe-H(8)A	139.9(4)
P(3)-Fe-C(1)	94.67(5)	P(2)-Fe-H(4)B	165.8(4)
Fe-P(1)-O(11)	121.78(5)	Fe-P(2)-O(23)	120.13(5)
Fe-P(1)-O(12)	118.41(5)	Fe-P(3)-O(31)	122.31(5)
Fe-P(1)-O(13)	115.39(5)	Fe-P(3)-O(32)	113.16(5)
Fe-P(2)-O(21)	123.39(5)	Fe-P(3)-O(33)	122.78(5)
Fe-P(2)-O(22)	111.60(5)		
C(1)-C(2)-C(3)	123.1(2)	C(1)-C(8)-H(8)B	110(1)
C(2)-C(1)-C(8)	123.2(2)	C(7)-C(8)-H(8)A	108(1)
C(2)-C(3)-C(4)	123.6(2)	C(7)-C(8)-H(8)A	107(1)
C(1)-C(8)-C(7)	114.1(1)	H(8)A-C(8)-H(8)B	103(2)
C(3)-C(4)-C(5)	114.2(2)	C(5)-C(4)-H(4)A	106(1)
C(6)-C(7)-C(8)	117.4(2)	C(5)-C(4)-H(4)B	109(1)
C(4)-C(5)-C(6)	116.9(2)	C(3)-C(4)-H(4)A	106(1)
C(5)-C(6)-C(7)	117.5(2)	C(3)-C(4)-H(4)B	110(1)
C(1)-C(2)-H(2)	117(1)	H(4)A-C(4)-H(4)B	111(2)
C(3)-C(2)-H(2)	119(1)	C(2)-C(3)-H(3)	115(1)
C(2)-C(1)-H(1)	114(1)	C(4)-C(3)-H(3)	114(1)
C(8)-C(1)-H(1)	114(1)	C(8)-H(8)A-Fe	86(1)
C(1)-C(8)-H(8)A	115(1)	C(4)-H(4)B-Fe	93(1)
	Torsion Angles (deg)		
C(2)-C(1)-C(8)-C(7)	52.2	C(6)-C(5)-C(4)-C(3)	41.8
C(5)-C(4)-C(3)-C(2)	−61.5	C(8)-C(7)-C(6)-C(5)	−52.0
C(2)-C(1)-C(8)-H(8)A	−72.8	C(7)-C(6)-C(5)-C(4)	62.6
H(4)B-C(4)-C(3)-C(2)	61.7	C(4)-C(3)-C(2)-C(1)	−36.0
C(1)-C(8)-C(7)-C(6)	−53.7	C(3)-C(2)-C(1)-C(8)	46.4

tively saturated system, **3**. The bonding involved in these M-H interactions will be discussed in the next section.

The Fe-H_{4B} interaction and resultant differentiation of the two basal phosphorus ligands provide an explanation for the previously mentioned ESR results.[6] The slow exchange spectrum displays hyperfine structure due to three nonequivalent phosphorus nuclei, consistent with the solid-state structure. A high-energy process, attributed to a turnstile motion of the three phosphorus ligands, equilibrates all three nuclei. A lower energy process equilibrates the two basal ligands, leaving the axial ligand unchanged. The low-energy process now can be attributed to exchange of the hydrogen atoms H_{4B} and H_{8A} in a process analogous to that observed in **1**. Hydrogen atom H_{8A} is too far from the iron center (3.08 (2) Å) for any interaction but can move closer to the iron center as H_{4B} moves away. The entire process requires only a low activation energy.

When considered independently from the rest of the molecule, the η^3-cyclooctenyl group, especially the allylic portion, appears relatively symmetrical. Bond distances and angles related by an imaginary plane passing through C_2 and C_6 of the boat conformation are all essentially equal. The allyl distances C_1-C_2 and C_2-C_3, at 1.419 (2) and 1.410 (2) Å, respectively, are very similar to those observed in **1** and **3** (1.407 (4) and 1.403 (4)° for **1** and 1.408 (5) and 1.397 (5)° for **3**). The central C-C-C angles of the allyl groups in **1**, **2**, and **3** are also very similar (C_1-C_2-C_3 = 122.0 (4), 123.1 (2), and 119.0 (3)°, respectively). The anti allylic angles in **2** are equal to each other (C_8-C_1-C_2 = 123.2 (2) and C_2-C_3-C_4 = 123.6 (2)°) and to those observed in **3**. This is in contrast to the nonequivalence observed in **1** (corresponding angles = 127.2 (4) and 117.9 (4)°). Remaining angles around the ring range from 114.1 (1) to 117.5 (2)°.

The first indication of asymmetry in the ring comes from

the related pairs of torsional angles about the ring. Each angle differs from its mirror-related counterpart by about 10°. In **1** the differences in related torsional angles range from 32 to 40° while the greatest difference in **3** is 2°. For subsequent discussion, the most significant pair of torsion angles is that involved with the allyl group: C_1-C_2-C_3-C_4 and C_8-C_1-C_2-C_3 are 16.4 and −52.9° for **1**, 36.0 and −46.4° for **2**, and 45.4 and −45.6° for **3**. Thus, in going from **1** to **2** to **3**, the interacting C-H group is swung away from the metal center as the ring becomes more symmetrical.

The bonding of the cyclooctenyl group to the FeP_3 fragment in **2** is clearly unsymmetrical. The view of **2** in Figure 3 shows the twisting of the allyl fragment relative to the three phosphite ligands. Additionally, C_3 is closer to Fe than C_1 (2.135 (2) vs. 2.170 (2) Å). The related distances in the very unsymmetrical 16-electron system, **1**, are 2.037 (3) and 2.161 (3) Å, while in **3** these distances are nearly equal at 2.113 (3) and 2.125 (3) Å. The skewing of the boat and shortening of Fe-C_3 both serve to bring H_{4B} closer to the iron center. The twisting of the cyclooctenyl group relative to the three phosphorus atoms brings H_{4B} into a position somewhat trans to P_2 (H_{4B}-Fe-P_2 = 165.8 (4)°). The trans P-Fe-H angle in **3** was 176.8 (3)°. The cis P-Fe-H_{4B} angles are 88.8 (4) and 94.0 (4)° (P_1 and P_2, respectively), while the related angles in **1** are 93.5 (3) and 89.1 (3)°. There are no comparable angles in **3** because there is no metal-hydrogen interaction.

Results and Discussion of the MO Calculations

The Model. In the cyclooctenyl-metal complexes, **1–3**, discussed above, the important metal to hydrocarbon interactions and changes in geometry involve primarily the three allylic carbon atoms and those atoms attached to them. Though it does not account for the additional conformational pressures of a ring, an *anti*-butenyl group was chosen as a model for the cyclooctenyl fragment. In an attempt to differentiate the allylic and methyl C-H contributions to the interaction between metal and the *anti*-butenyl group, the propenyl and *syn*-butenyl analogues were studied also. Calculations were carried out on the model compounds $[M(\eta^3\text{-alkenyl})(PH_3)_3]^y$ (M = Co, y = molecular charge = 0, 1+, 2+; M = Fe, y = 0, 1+; alkenyl = propenyl, *syn*- and *anti*-butenyl). There were no significant differences between the results calculated for the iron complexes and their isoelectronic cobalt analogues. Therefore, for simplicity, we refer hereafter only to the cobalt calculations. Calculations involving the cobalt complexes with molecular charge 2+, 1+, and 0 are model complexes for **1**, **2**, and **3**, respectively, and are hereafter referred to as **M1**, **M2**, and **M3**. It should be pointed out that these complexes are d^6, d^7, and d^8, respectively, and in the absence of any metal-hydrogen interaction they are 16-, 17-, and 18-electron systems.

Optimization of Geometry. The geometries of the complexes are defined with respect to an axis passing through Co and an arbitrary point, X (see schematic **4**). Preliminary calculations

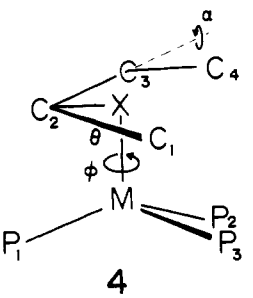

4

with the three PH_3 groups placed symmetrically about the axis and the allyl group in a plane perpendicular to the axis showed that small variations in phosphine orientation were energetically relatively unimportant. Therefore, in subsequent optimizations the $[Co(PH_3)_3]$ fragment was held rigid with Co-P = 2.15 Å, P-H = 1.40 Å, ∠Co-P-H = 115°, and ∠X-Co-P = 125°, which corresponds to ∠P-Co-P = 90.4°. The η^3-propenyl fragment [C_1-C_2-C_3] was fixed with the carbon and hydrogen atoms coplanar (C-C = 1.42 Å, C-H = 1.10 Å, ∠CCH = ∠C-C-C = 120°). For the *syn*- and *anti*-butenyl calculations, the appropriate hydrogen atoms on C_3 were replaced by a methyl group (C_4) with C_3-C_4 = 1.56 Å. In separate calculations, the torsion angle C_1-C_2-C_3-C_4, α, was both varied and fixed at 0 (anti), 180 (syn), and 35° (for positive angles <180° C_4 is above the plane of the allyl group in configuration **4**). The bonding of these fragments to Co was optimized through variation of the Co-X and X-C_2 distances and the angles θ and ϕ. In certain calculations, the torsion angle, α, was also varied. The alkenyl rotation angle, ϕ (defined as the torsion angle P_1-Co-X-C_2), was rotated stepwise in 10° increments for the calculation of rotational barriers.

The optimized geometries of the model complexes, **M1, M2,** and **M3,** are compared with selected experimental parameters of the cyclooctenyl complexes **1, 2,** and **3,** in Table III. Columns 1 and 2 show bond lengths and angles for the propenyl and η^3-*syn*-butenyl complexes which define their orientation with respect to the $[Co(PH_3)_3]$ fragment. Column 4 contains results for the η^3-*anti*-butenyl complexes where α was allowed to vary and column 3 contains results for the η^3-*anti*-butenyl complex where α was set at 35° for reasons discussed below. Note that the variables defined above require that Co-C_1 and Co-C_3 distances be equal at all times.

The optimized geometries of the *anti*-butenyl complexes duplicate the important aspects of the crystallographically determined structures remarkably well. The orientation of the allylic group with respect to the phosphorus ligands is reproduced in each case, with C_2 eclipsing P_1 in **M1** and **M2** but not in **M3** (ϕ = 60°). The metal to hydrocarbon distances are reasonable and in many cases accurate to within a few hundredths of an ångstrom. Most deviations from the observed structures may be rationalized in terms of the shortcomings of the models. Obviously, an η^3-*anti*-butenyl group cannot "feel" the additional conformational pressures of an eight-carbon cyclic system. The cyclooctenyl ring in **1** has contorted with C_1 away from and C_3 toward the metal maximizing the C_4-H-M interaction. This contortion was not allowed in the model, but nonetheless the C_4-H-M interaction is maintained. The torsion angle α optimized at 0°, suggesting some butadiene character in the four-carbon fragment. The optimization was not prejudiced by shortening the C_3-C_4 bond from 1.56 to 1.48 Å as found in the crystal structure of **1**.[9] Nevertheless, the methyl-group orientation is very close to the position of the corresponding methylene group in **1**. In comparing the **M2** *anti*-butenyl complex with **2**, we find that allowing the torsion angle α to vary gives reasonable results with respect to the allylic carbon atoms but the calculated position of the methyl group is too close to the metal center (see columns 4 and 5, Table III). If the large torsion angle observed experimentally (36.0°) is assumed to be a result of conformational pressures of the ring, it is reasonable to fix α at 35°. When this is done, better agreement is found (columns 3 and 5), especially for the methyl group position. A similar result is found in comparing the 18-electron systems, **M3** and **3** (columns 3 and 5).

A comparison of the models reveals that *the ground-state orientation of the allylic unit is relatively unaffected by the presence or orientation of a methyl group in any of the three oxidation states.* This provides the first clue that, while M-H-C_4 interactions are observed in **1** and **2**, the bonding of the allylic unit to $[M(PH_3)_3]$ dominates the orientation of the four-carbon fragment.

Allyl-Metal Bonding. Albright, Hofmann, and Hoffmann[20] have presented a thorough analysis of the bonding between

Table III. Experimental and Calculated Geometric Parameters for 16-, 17-, and 18-Electron M(η^3-alkenyl)L_3 Complexes[b]

	propenyl	*syn*-butenyl	*anti*-butenyl		expt1
			α fixed	α varied	(cyclooctenyl)
		d^6 Complexes—16-Electron—**1**			
rotation ϕ	0	0	0	15.1	15[a]
M-C(1)	2.19	2.18	2.12	2.16	2.17
M-C(2)	2.05	2.04	2.09	2.06	2.08
M-C(3)	2.19	2.18	2.12	2.16	2.05
M-C(4)			2.83	2.43	2.37
M-H			2.54	1.90	1.88
torsion α			35[a]	0	16.4
∠P(1)-M-C(2)	90.2	91.2	91.9	90.7	91.5
		d^7 Complexes—17-Electron—**2**			
rotation ϕ	0	0	0	6.3	15[a]
M-C(1)	2.21	2.21	2.15	2.19	2.17
M-C(2)	2.05	2.04	2.07	2.05	2.03
M-C(3)	2.21	2.21	2.15	2.19	2.14
M-C(4)			2.94	2.65	2.98
M-H			2.69	2.20	2.77
torsion α			35[a]	8.8	36.0
∠P(1)-M-C(2)	94.2	96.8	94.8	94.8	95.8
		d^8 Complexes—18-Electron—**3**			
rotation ϕ	180	180	180	180	175[a]
M-C(1)	2.22	2.22	2.16	2.20	2.13
M-C(2)	2.02	2.02	2.02	2.01	1.96
M-C(3)	2.22	2.22	2.16	2.20	2.11
M-C(4)			3.07	2.93	
M-H			2.87	2.62	
torsion α			35[a]	20	45
∠P(1)-M-C(2)	134.0	133.3	134.3	138.5	130

[a] Determined graphically; there is no equivalent number from structural results. [b] Bond lengths in ångstroms, angles in degrees.

$M(CO)_3$ and polyene fragments showing the changes caused by changing ϕ from 0 to 60°. The same analysis applies to the $[M(\eta^3\text{-}C_3H_5)(PH_3)_3]$ system discussed here. The modification in bonding that occurs upon rotating the allyl group is related primarily to changes in two molecular orbitals. Figure 4 compares the frontier molecular orbitals for $M(C_3H_5)L_3$ at ϕ = 0 and 60° (or 180°); a schematic representation of the change in overlap between metal and allyl unit is shown for orbitals A and D. Lower energy orbitals change little in these two orientations and the differences tend to cancel each other. For **M1**, the highest occupied molecular orbital (HOMO) is C. The change in orbital A on going from eclipsed to staggered orientation causes destabilization of the orbital (~0.2 eV) through loss of bonding overlap. Therefore, in **M1** the eclipsed orientation (ϕ = 0°) will be stabilized by about 0.4 eV (~9.6 kcal/mol). In **M3**, two electrons have been added to orbital D. The stability gained in orbital D (~0.3 eV) in the staggered orientation (ϕ = 60°) is more than enough to offset the destabilization of orbital A, and the complex adopts a geometry with ϕ = 60°. The 17-electron system **M2** is intermediate between **M1** and **M3** in that only one electron is placed in orbital D. The added stability of one electron in orbital D at ϕ = 60° is not enough to offset the two electrons in orbital A so the eclipsed geometry is retained, but the difference in stability between the two geometries is small.

C–H to M Interaction. Having established that the overall orientation of the hydrocarbon fragment is dominated by the allyl–metal interaction, the degree and significance of the M–H–C_4 interaction are now discussed. The optimized geometry of the *anti*-butenyl **M1** complex (and crystallographic structure of **1**) suggests significant interaction between M, H, and C_4. The molecular orbital wave functions reveal that only one of the filled orbitals has significant C_4, H, and M coefficients. The orbital is relatively low in energy and consists primarily of allylic π interaction. Figure 5a illustrates a three-dimensional contour of a constant surface calculated for 0.05

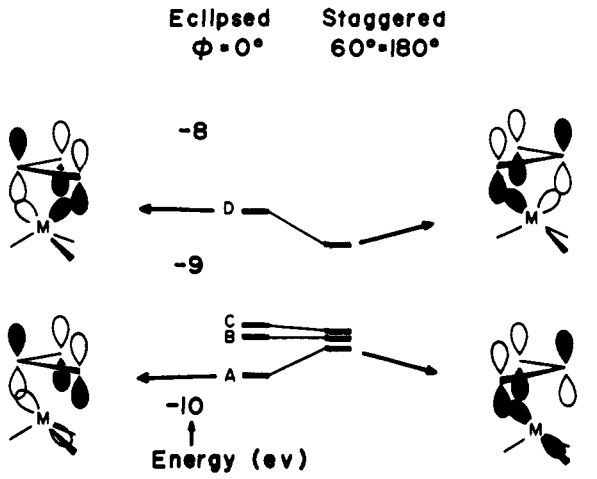

Figure 4. Frontier molecular orbital energy level diagram for the M(η^3-propenyl)$(PH_3)_3$ system for angle ϕ between 0 and 60°. Schematic representation of the change in overlap between metal and allyl is shown for orbitals A and D. Orbitals A, B, and C are filled for the d^6 system with additional electrons going into orbital D.

electron. The methyl contribution is a combination of a C_4 p orbital with two hydrogen s orbitals which constructively interact with a weak metal d orbital and a phosphorus donor orbital. Disregarding the predominant allyl π bonding, the metal–methyl interaction is best described as a three-center [Co–H–C_4], two-electron bond as opposed to either a metal–hydrogen or metal–carbon interaction.

The lowest unfilled molecular orbital (LUMO) of **M1** also contains a Co–H–C_4 interaction illustrated in Figure 5b. The metal and phosphorus contributions are larger and antibonding with respect to each other. More significantly, the interaction between M and C_4–H is antibonding as is the C_4–C_3 interaction, while the C_4–H interaction is bonding in nature.

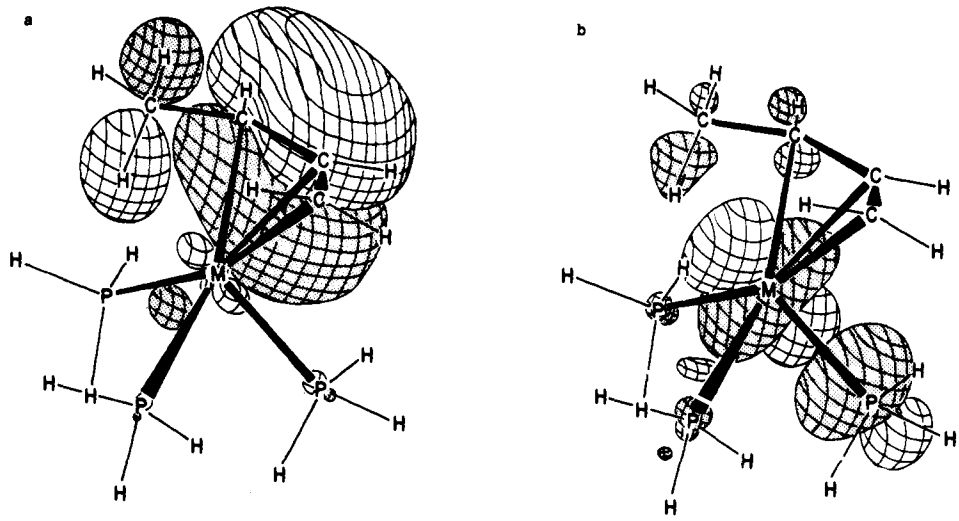

Figure 5. Three-dimensional contours of the charge envelopes calculated at 0.05 electron for (a) the major C–H–M bonding orbital and (b) the lowest unoccupied molecular orbital in the d^6 M(η^3-butenyl)$(PH_3)_3$ system.

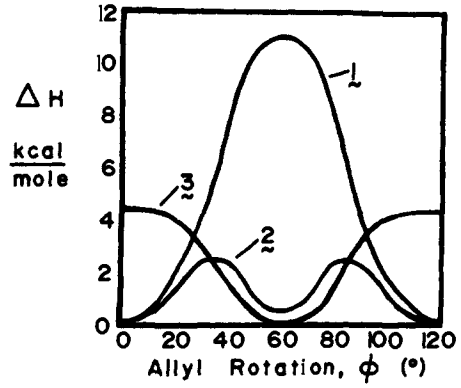

Figure 6. Calculated energy profiles for the d^6, d^7, and d^8 electron systems, **M1**, **M2**, and **M3** as a function of angle ϕ (see text and configuration **4**).

This orbital is important in the analysis of the Co–H–C_4 interaction in **M2**. While the weak bonding interaction described above for the filled orbital would still be available, the addition of one electron to the LUMO (in which the antibonding interaction between M and C–H seems to be more significant than the related M to C–H bonding interaction in the filled orbital) would destabilize the metal to methyl C–H bonding interaction. When the torsion angle, α, was allowed to optimize for **M2**, it increased, moving the methyl group away from the metal center (see Table III, column 4). In **2**, the torsion angle is even greater than the optimized value, but this discrepancy may be attributed to ring conformation. In **M3**, the effect of another electron in the LUMO increases the torsion angle, α, again, increasing the methyl to metal distance even more.

The relative magnitude of Co–C(4) and Co–H interactions can be estimated from the molecular energies calculated for the optimized geometries and those in which the methyl torsion angle, α, was fixed at 35°. Using **M3** with ϕ constrained to 0° as a base where no constructive Co–H–C_4 interaction exists, 5.1 kcal/mol must be applied to change α from the optimized value (20°) to 35°. For **M2**, the change in α from optimum (8.8°) to 35° requires 6.1 kcal/mol while 13.1 kcal/mol is required for **M1**. Therefore, the M to C–H interactions in **M2** and **M1** are stronger than that in **M3** by about 1 and 8 kcal/mol, respectively. Interestingly, if the methyl group is rotated by 60° so that the hydrogen to metal interaction is minimized while maintaining a possible M–C_4 interaction, the **M1** complex is destabilized by about 2.5 kcal/mol, while **M2** and **M3** are both stabilized slightly. The additional stability in the latter cases indicates a repulsive nature for the Co–H interaction. However, as models of the cyclooctenyl system, the nonrotated methyls are more accurate because the conformation of the ring does not allow a rotation of these hydrogen atoms to minimize interaction.

Fluxional Motion. Allyl Rotation. Having established that the calculations successfully model the ground-state geometries in the **M1**, **M2**, and **M3** systems, we now model an allyl rotation profile and obtain the barriers to rotation. Using a simplistic approach, the $[Co(PH_3)_3]$ fragment was held rigid. This of course does not allow consideration of a Berry pseudorotation pathway. The orientation of the allylic or butenyl fragment was reoptimized for fixed values of ϕ from $\phi = 0$ to 120° in 10° increments.

Rotation of the η^3-propenyl group in **M3** is accompanied by variations of the angle, θ, and the M–X and X–C_2 distances. While the M–C_2 and M–C_1 (M–C_3) distances are relatively constant at 2.04 and 2.22 Å, respectively, the C–X distance varies from 0.85 Å at $\phi = 0°$ to 0.33 Å at $\phi = 60°$, the ground-state configuration. Carbon C_2 moves down toward the phosphorus nuclei as they are eclipsed.

Much the same rotational behavior is observed in **M2**, but the amplitude of motion is much greater. The distance X–C_2 varies from 1.05 Å for $\phi = 0°$, the ground state, to 0.02 Å at $\phi = 60°$. As in **M3**, the M–C_2 and M–C_1 (M–C_3) distances remain relatively constant around 2.05 and 2.21 ϕ, respectively. This constancy of the metal–carbon distances during fluxional behavior and upon changing from an 18- to a 17-electron system is surprising; the metal center can be viewed as a hard sphere with the propenyl group sliding on its surface.

Fluxional behavior in the **M1** propenyl complex is slightly different in that the movements are of smaller magnitude. Additionally, the M–C_2 distance varies from 2.05 Å at $\phi = 0°$ to 2.14 Å at $\phi = 60°$, while the M–C_1 and M–C_3 distances remain constant at 2.18 Å.

The rotation of an η^3-*syn*-butenyl group gives results very similar to those with the propenyl group. The simulations involving the η^3-*anti*-butenyl group, though similar in nature, showed dampening in the amplitude of motions.

The differences in molecular energy calculated for the rotational profile discussed above give an estimate of the change in enthalpy of rotation ($\Delta H^{\ddagger}_{rot}$). The calculated values for **M1**, **M2**, and **M3** and the spectroscopically determined values for

Table IV. Barriers to Alkenyl Group Rotation in 16-, 17-, and 18-Electron (η^3-alkenyl)ML_3 Complexes

	$\Delta H^{\ddagger}$, kcal/mol				
			anti-butenyl		exptl
	allyl	*syn*-butenyl	α fixed	α varied	(cyclooctenyl)
M1	11	11	10	12	**1** 16.5
M2	2	2	3	6	**2** 4.6
M3	4	4	6	5	**3** ~6

1, 2, and **3** are given in Table IV; the five columns correspond to the same species as in Table III. The barriers to rotation for the first three models are qualitatively correct in their positions relative to each other when compared with experimental. When the torsion angle, α, in the *anti*-butenyl species is allowed to vary, the barriers for **M1** and **M3** vary little, but the barrier for **M2** increases dramatically. This result suggests that, while $Fe(\eta^3\text{-}C_3H_5)(P(OMe)_3)_3$ and its η^3-*syn*-butenyl analogue should have rotational barriers similar to those of **2**, $Fe(\eta^3$-*anti*-butenyl$)(P(OMe)_3)_3$ may have a higher barrier to rotation.

The calculated energy profile for **M1, M2,** and **M3** as the propenyl group is rotated through 120° is plotted in Figure 6. While **M1** and **M3** have the expected bell-shaped curves, the plot of **M2** resembles a linear combination of the other two with minima at ϕ = 0 and 60° and maxima between 30–40 and 80–90°. This plot illustrates that the nature of the 17-electron complex is intermediate between those of the 16-electron and 18-electron complexes. The plot also gives an indication why the 17-electron complex is fluxionally more labile than the other two. The minima of **M2** correspond to square-pyramidal geometries whereas the maxima are at the points of greatest distortion from square-pyramidal geometry.

The propenyl 16-electron complex has not yet been isolated in the absence of an M–H–C interaction; $M(\eta^3\text{-}C_3H_5)L_4$ are isolated when M is a d^6 metal.[5] In these complexes a static structure is observed by NMR, suggesting a barrier to rotation in these "octahedral" complexes of >20 kcal/mol. We briefly examined the fluxional behavior of this allylic species allowing the angular disposition of the phosphines to independently vary during rotation as shown in the schematic **5.** The barrier was

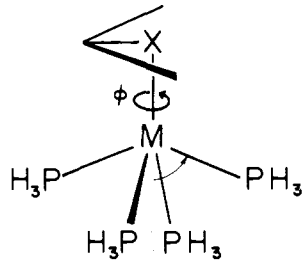

5

calculated to be $\Delta H^{\ddagger}_{rot}$ = 19.6 kcal/mol with a minimum at ϕ = 0° and a maximum at ϕ = 45° where all the PH_3 groups were symmetrically oriented. This motion has been discussed more thoroughly by Albright, Hoffmann, Tse, and D'Ottavio.[21]

Conclusions

The foregoing structural and computational results, when considered with previous spectroscopic[5] and structural[9] results, indicate that the C–H to M interaction in $[Fe(\eta^3\text{-}C_8H_{13})(P(OMe)_3)_3]^+$ (**1**) is an open C–H–M three-center–two-electron bond, having an additional interaction with the entire π-enyl system. The bond is a modification of the closed 2e–3c bond originally proposed for a closely related system by Brookhart, Whitesides, and Crockett.[22] Addition of one electron to **1** greatly weakens the C–H to M interaction (as in **2**), but it persists until the addition of a second electron to the metal center. At that point there is no indication of any C–H to M interaction. For **1** and **2** the C–H–M interaction serves as an additional stabilizing influence in the coordinatively unsaturated species, but the overall geometries of the complexes are determined primarily by the metal–allyl bonding.

The fluxional processes occurring in complexes **1**[5] and **2**[6] are very similar in nature, their major difference being their activation parameters. In both cases, the higher energy process involves mutual exchange of all three phosphorus nuclei. Both **1** and **2** have C_4–H–M interactions in a sixth coordination site. In both cases, the lower energy exchange process can be attributed to exchange of C_8–H for C_4–H in the C–H–M interaction. The exchange of the two hydrogen atoms equilibrates the two sides of the cyclooctenyl ring, and thus the environments of the two equatorial phosphorus nuclei, accounting for their apparent exchange.

Acknowledgments. We wish to acknowledge a debt of gratitude to Dr. D. A. Pensak for allowing us to use his TRIBBLE SYSTEM prior to publication. We also are indebted to Professors Victor Day, Earl Muetterties, and Roald Hoffmann for results prior to publication. We also gratefully acknowledge the fine technical assistance of Messrs. L. Lardear and M. A. Cushing, Jr. Discussions of the Hückel calculations with Dr. F. A. Van-Catledge have been of great value.

Supplementary Material Available: Listings of observed and calculated structure factors as well as tables of anisotropic thermal parameters for the nonhydrogen atoms and coordinates for hydrogen atoms (40 pages). Ordering information is given on any current masthead page.

References and Notes

(1) H. D. Murdoch and E. A. C. Lucken, *Helv. Chim. Acta*, **47**, 1517 (1964).
(2) E. L. Muetterties, B. A. Sosinsky, and K. I. Samaraev, *J. Am. Chem. Soc.*, **97**, 5299 (1975).
(3) C. F. Putnick, J. J. Welter, G. D. Stucky, M. J. D'Aniello, Jr., B. A. Sosinsky, J. F. Kirner, and E. L. Muetterties, *J. Am. Chem. Soc.*, **100**, 4107 (1978).
(4) S. D. Ittel, F. A. Van-Catledge, C. A. Tolman, and J. P. Jesson, *J. Am. Chem. Soc.*, **100**, 1317 (1978).
(5) S. D. Ittel, F. A. Van-Catledge, and J. P. Jesson, *J. Am. Chem. Soc.*, **101**, 6905 (1979).
(6) S. D. Ittel, P. J. Krusic, and P. Meakin, *J. Am. Chem. Soc.*, **100**, 3264 (1978).
(7) ^{31}P hyperfine couplings = 99.6, −27.9, and −10.5 G.
(8) V. Day and E. L. Muetterties, private communication.
(9) (a) J. M. Williams, R. K. Brown, A. J. Schultz, G. D. Stucky, and S. D. Ittel, *J. Am. Chem. Soc.*, **100**, 7407 (1978); (b) J. M. Williams, R. K. Brown, A. J. Schultz, G. D. Stucky, S. D. Ittel, and R. L. Harlow, *ibid.*, submitted.
(10) The theory derived by A. Anderson (*J. Chem. Phys.*, **62**, 1187 (1975)) is similar to extended Hückel theory but includes a correction for two-body repulsion. It has been applied to the interaction of small molecules with metal clusters and surfaces as well as with a few organometallic derivatives (A. B. Anderson, *J. Am. Chem. Soc.*, **100**, 1153 (1978), and references cited therein; *Inorg. Chem.*, **15**, 2598 (1976)). The parameter set and examples of the application of this technique to optimize transition metal carbonyl bonding are found in D. A. Pensak and R. J. McKinney, *ibid.*, in press.
(11) S. D. Ittel, F. A. Van-Catledge, and J. P. Jesson, *J. Am. Chem. Soc.*, **101**, 3874 (1979).
(12) B. A. Frenz, "The Enraf-Nonius CAD 4 SDP—A Realtime System for Concurrent X-ray Data Collection and Crystal Structure Determination", in "Computing in Crystallography", H. Schenk, R. Olthof-Hazekamp, H. vanKoningsveld, and G. C. Bassi, Eds., Delft University Press, Delft, Holland, 1978, pp 64–71.
(13) "International Tables for X-ray Crystallography", Vol. IV, Kynoch Press, Birmingham, England, 1974: (a) Table 2.2B; (b) Table 2.3.2.
(14) P. W. R. Corfield, R. J. Doedens, and J. A. Ibers, *Inorg. Chem.*, **6**, 197 (1967).
(15) See paragraph at end of paper regarding supplementary material.
(16) E. Clementi and P. L. Raimondi, *J. Chem. Phys.*, **38**, 2686 (1963); E. Clementi, D. L. Raimondi, and W. P. Reinhardt, *ibid.*, **46**, 1300 (1967).
(17) J. W. Richardson, W. C. Nieuwpoort, P. R. Powell, and W. F. Edgell, *J. Chem. Phys.*, **36**, 1047 (1962); J. W. Richardson, R. R. Powell, and W. C. Nieuwpoort, *ibid.*, **38**, 796 (1963).

(18) W. Lolz, *J. Opt. Soc. Am.*, **60**, 206 (1970).
(19) For instance, see ref 11–16 of ref 9b.
(20) T. A. Albrighl, P. Hofmann, and R. Hoffmann, *J. Am. Chem. Soc.*, **99**, 7546 (1977).
(21) T. A. Albrighl, R. Hoffmann, Y. Tse, and T. D'Ottavio, *J. Am. Chem. Soc.*, **101**, 3812 (1979).
(22) M. Brookhart, T. H. Whitesides, and J. M. Crockett, *Inorg. Chem.*, **15**, 1550 (1976).

Coordination Chemistry of 7,9-Disubstituted 6-Oxopurine Metal Compounds. 1. Copper(II) Coordination at N(1). Molecular and Crystal Structure of (Glycylglycinato)(7,9-dimethylhypoxanthine)copper(II) Tetrahydrate

Luigi G. Marzilli,* Kenneth Wilkowski, Chian C. Chiang, and Thomas J. Kistenmacher*

Contribution from the Department of Chemistry, The Johns Hopkins University, Baltimore, Maryland 21218. *Received April 18, 1979*

Abstract: The synthesis, ^{1}H NMR line broadening, and molecular and crystal structure of the complex (glycylglycinato)(7,9-dimethylhypoxanthine)copper(II), $Cu(ON_4C_7H_8)(O_3N_2C_4H_6)$, are reported. The complex crystallizes as the tetrahydrate in the orthorhombic system, space group $P2_12_12_1$, with a = 14.314 (6) Å, b = 7.741 (2) Å, c = 16.032 (6) Å, V = 1776.4 Å^3, Z = 4, d_{measd} = 1.62 (1) g cm^{-3}, d_{calcd} = 1.61 g cm^{-3}. Intensities for 2841 symmetry-averaged reflections were collected in the θ-2θ scan mode on an automated diffractometer employing graphite-monochromatized Mo Kα radiation. The structure was solved by standard heavy-atom Patterson and Fourier methods. Full-matrix least-squares refinement has led to a final R value of 0.036, a final weighted R value of 0.039, and a goodness-of-fit value of 1.75. The absolute configuration of the structure has been established. The primary coordination sphere about the copper is approximately square planar with the tridentate glycylglycine dianion and N(1) of the 7,9-dimethylhypoxanthine ligand, Cu–N(1) = 1.977 (3) Å, occupying the four coordination sites. In addition to the strongly coordinated equatorial plane, the copper also forms two weak, axial interactions with O(6) of the 7,9-dimethylhypoxanthine ligand: one intramolecular, Cu–O(6) = 2.970 (2) Å, and one intermolecular, Cu–O(6) = 2.769 (2) Å. The coordination geometry displayed is very similar to that observed in a variety of copper(II) complexes with N(3)-coordinated cytosine derivatives as ligands. The crystal structure is dominated by helical arrays of complexes, stabilized by the intermolecular Cu–O(6) interaction, and of hydrogen-bonded water molecules about twofold screw axes parallel to the crystallographic b axis. ^{1}H NMR line-broadening data in H_2O suggest that N(1) is the primary coordination site for Cu(II) in solution. It seems probable that the N(1),O(6) grouping may have a similar coordination chemistry to the N(3),O(2) grouping of cytosine in N(1)-substituted cytosine derivatives.

Introduction

Beginning in the early part of this decade, a number of investigators began to study the details of the binding of metal species to nucleic acid components.[1] This activity was motivated in large part by the known influence of metal species on the biochemistry and structure of nucleic acids[2] and by the likely involvement of such interactions in the mode of action of the important metalloantineoplastic drugs based on and including *cis*-($Pt^{II}(NH_3)_2Cl_2$).[3] Rosenberg[3] has summarized current speculation on the mechanism of action of the platinum antitumor agents. Binding to the 6-oxopurine base in guanosine is frequently cited as being involved in the important lesion. In turn, two diverse classes of possibilities have been put forward which involve binding to the purine base and which provide a possible explanation for the antitumor activity of cis but not trans isomers of the type $Pt^{II}(ammine)_2Cl_2$. The first type of explanation invokes intrastrand cross-linking between adjacent guanosine bases with the Pt binding exclusively to N(7) of the purine base.[4] Good structural models for such compounds have been studied.[5-7] The second type of explanation invokes participation of the 6-oxo group in binding to the metal.[8] Repair enzymes act relatively slowly on 6-oxo alkylated guanosine in DNA.[9] There is general agreement that monodentate coordination of the 6-oxo group to a metal will be quite unstable and that involvement of the 6-oxo group would require chelation. Most workers favoring chelate complex formation have championed the controversial suggestion that N(7),O(6) chelation is involved.[10-12] However, consideration of the geometry required for such chelation has led many to suggest that such a structure is unlikely.[1] A bonding arrangement which is more feasible and for which there is some precedence involves N(1),O(6) chelation.[13]

In past studies, we have evaluated the feasibility of the N(7),O(6) chelation mode by investigating Cu(II) Schiff base complexes.[14,15] The versatility of the Cu(II) center in forming long axial bonds permitted the isolation and structural characterization of the only established example of a complex exhibiting the controversial N(7),O(6) chelation mode,[14] albeit the Cu–O(6) interaction is weak. In this study, we extend this approach and report the preparation and structure of a Cu(II) complex containing an N(1)-bound 6-oxopurine, namely, [(glycylglycinato)(7,9-dimethylhypoxanthine)copper(II)]-tetrahydrate. To our knowledge, this is the first structural study of such a compound with any metal species, although the N(1) bonding mode is well established in solution.[1]

Experimental Section

The title complex was prepared by the addition of 7,9-dimethylhypoxanthine[16] (0.85 g, 5 mmol) dissolved in a minimum amount of H_2O and hydrated glycylglycinatocopper(II)[17] (1.1 g, 5 mmol) in

0002-7863/79/1501-7504$01.00/0 © 1979 American Chemical Society